

Analysis of the spiral structure in a simulated galaxy

Mata-Chávez, M. Dolores,¹ ^{*}, Gómez, Gilberto C.¹, and Puerari, Ivânio²

¹Centro de Radioastronomía y Astrofísica, Universidad Nacional Autónoma de México, Apdo. Postal 3-72, Morelia Mich. 58089, México

²Instituto Nacional de Astrofísica, Óptica y Electrónica, Calle Luis Enrique Erro 1, 72840 Santa María Tonantzintla, Puebla, México

13 October 2018

ABSTRACT

We analyze the spiral structure that results in a numerical simulation of a galactic disk with stellar and gaseous components evolving in a potential that includes an axisymmetric halo and bulge. We perform a second simulation without the gas component to observe how it affects the spiral structure in the disk. To quantify this, we use a Fourier analysis and obtain values for the pitch angle and the velocity of the self-excited spiral pattern of the disk. The results show a tighter spiral in the simulation with gaseous component. The spiral structure is consistent with a superposition of waves, each with a constant pattern velocity in given radial ranges.

Key words: Galactic: disc – Galactic: structure

1 INTRODUCTION

The spiral structure of disk galaxies has been studied for many years now, yet the origin of this structure remains uncertain. Several different theories have been proposed to explain how this structure was formed. The density wave theory (Lin & Shu 1964; Bertin & Lin 1996) proposes quasi-stationary density waves propagating through a rotating disk at constant pattern angular velocity. As an alternative, the Swing Amplification Theory (Goldreich & Lynden-Bell 1965; Julian & Toomre 1966) proposes that the arms arise from smaller perturbs (or perturbations) which add and amplify. This could produce over-densities rotating with the disk. In this model waves are not quasi-stationary and, therefore when the perturbs ceases the spiral disappears. D’Onghia et al. (2013) showed that over-densities could produce non-linear effects in swing amplifications that modify the formation and longevity of the spiral pattern, even after the perturbations have been removed.

In order to study these scenarios, researchers have used N-body simulations. These have been able to reproduce a spiral like structure generated in many different ways, such as interaction with other galaxies or gravitational instabilities in the disk. Most of these simulations involve a stellar disk only (Grand et al. 2012a,b; Roca-Fàbrega et al. 2013; Quillen et al. 2011), yet the spiral structure is conspicuous in the gaseous component also (Acreman et al. 2010). Vallée (2005, and references therein) showed that the Galactic stellar spiral structure differs from the gaseous one (see also Gómez et al. 2013).

Recently, Wada et al. (2011) and Baba et al. (2013)

showed simulations with stellar and gaseous disks. In those studies, a spiral structure that seems to co-rotate with the galactic disk is formed.

Several methods have been developed to quantitatively describe the spiral structure in a galactic disk, either in observed images or in a numerical simulations. Using Fourier transformations of images of spiral galaxies, it is possible to obtain estimations of the pitch angle, relative strengths of modes and other parameters of the spiral structure (Davis et al. 2012).

But the issue of the gas role in the formation of the spiral pattern remains unsatisfactorily open. It is usually considered ((Bertin & Lin 1996; Sellwood & Carlberg 2014; Dobbs & Baba 2014), for example) that the principal role of the gas is to dynamically cool the stellar disk. Nevertheless, the large scale interaction of these components have not been properly explored since it is assumed that the small mass of the gaseous disk will have a negligible impact on the dynamics of the stellar one, and so the gaseous component is frequently considered as a perturbation, brushing aside the possible dynamical feedback on the large scale dynamics. In this paper, we compare the spiral structure of galactic disks with and without a gaseous component using 3D numerical simulations. We use Fourier transforms to measure the parameters of the spiral pattern of the disks. In §2 we describe the simulations performed. In §3 we present the analysis of the spiral structure in the simulations performed. Finally, we present a summary in §4.

* E-mail: m.mata@crya.unam.mx

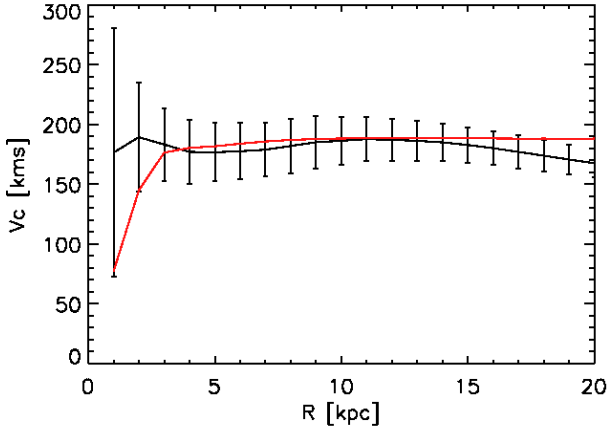


Figure 1. Mean rotational velocity of the simulation. The gray line corresponds to $t = 0$ Myr and black line at $t = 200$ Myr. The error bars show the standard deviation at different radii.

2 METHOD

Our simulation contains a galactic disk with $9.8 \times 10^8 M_{\odot}$ of gas and $3.49 \times 10^{10} M_{\odot}$ of stars. Both components are distributed initially with a constant midplane density of 0.62 and $0.017 M_{\odot}/\text{pc}^3$ for stars and gas, respectively, out to a radius of 3 kpc. Outside this radius, the midplane density follows an exponential profile $\rho = \rho_0 \exp[-(R - R_0)/R_h]$, with $R_0 = 8$ kpc, $\rho_0 = 0.15 M_{\odot}/\text{pc}^3$ and $R_h = 3.5$ kpc for the stellar disk, and $\rho_0 = 10^{-2} M_{\odot}/\text{pc}^3$ and $R_h = 8$ kpc for the gaseous disk. In the vertical direction, both components initially follow a Gaussian profile, with scale heights 0.325 and 0.135 kpc for stars and gas, respectively.

The particles in the galactic disk are setup in rotational equilibrium with a potential similar to that described in Allen & Santillan (1991), which consists in a halo, a bulge and a stellar disk (see fig. 1). In addition to the circular velocity, a velocity dispersion of 20 km s^{-1} is added to the stars, and of 12 km s^{-1} to the gas. The Toomre Q parameter for the disk is < 1 in the range $2 \text{ kpc} < R < 7 \text{ kpc}$.

The simulation is performed with the GADGET2 code (Springel et al. 2001), which solves the hydrodynamic equations using a SPH algorithm coupled to stellar dynamics. We used 6×10^6 stellar particles and 6×10^6 gas particles, randomly distributed over the disk following the density profile described above. The simulations are set up within a 40 kpc box. The version of the GADGET2 code we use have a sink particle formation prescription (Jappsen et al. 2005) with a critical density for sink formation of $3 \times 10^3 \text{ cm}^{-3}$.

Since the mass resolution is similar to the masses of giant molecular complexes, it is necessary to consider the gas segregation into phases. To achieve this, the simulation include the cooling function described in Koyama & Inutsuka (2000).¹ To avoid a prohibitively short time step, we apply the fast cooling model described in Vázquez-Semadeni et al. (2007), which evolves the gas temperature as exponentially

¹ Please note a typographical error in the expression for the cooling function in Koyama & Inutsuka (2000). See Vázquez-Semadeni et al. (2007).

approaching the equilibrium temperature at the current density. The segregation of the gas in phases, the dynamics of the dense clouds formed, and associated star formation, as modeled by sink particle formation, will be explored in a future work.

We performed two simulations. Simulation I consisted on both stellar and gaseous disk components, while simulation II consisted only on the stellar component, with the same random density and velocity distribution as the stellar disk in simulation I. Simulation I was evolved through 410 Myr, while we were able to evolve simulation II through 923 Myr. In both simulations, the particles start in an unrelaxed state, and so the self-stimulated spiral appears sooner than in relaxed simulations. Nevertheless, since the evolution lasts $3.5\tau_{rot}$ (where τ_{rot} is the rotation period at the stellar disk scale length, $\tau_{rot} = 120$ Myr), the evolution should be enough to erase signatures of the initial conditions.

Figure 2 shows mass surface density maps of the simulations at $t = 200$ Myr for the gaseous disk in simulation I (top) and stars (middle), and the stellar disk in simulation II (bottom). The galaxies in the simulations are not perturbed, so the spiral structure forms due to self-gravity out of the random fluctuations in the initial particle distribution. In simulation I, the gaseous and stellar disk have similar large scale structure, namely four spiral arms with basically the same locus, but the stellar arms are thicker than the gaseous ones, with the later showing much more substructure, as expected. But it is noticeable that the stellar arms in simulation I show more substructure than those in simulation II, the most noteworthy being a “hook” around $(x, y) = (-4, 7)$ kpc, although the overall strength of the arms differ in both simulations. The presence of a gaseous component is known to destabilize a disk (Jog 1996), since the gas is dissipative and is allowed to cool. But, we find that the stellar density in the arms is larger in simulation II, with the spiral arms remaining coherent longer (see §3).

3 SPIRAL STRUCTURE

Following Grand et al. (2012a), we describe the spiral structure in the simulations using a Fourier analysis of the mass surface density distributions of stars and gas. Consider the Fourier transform (along the azimuthal angle ϕ , at a given radius r) of the surface density distributions resulting from the simulations, $A(m, r)$, where m is the Fourier mode in question. Since both simulations develop four arms (see fig. 2), we show the time evolution of the $A(4, r)$ mode in Figure 3. It can be seen that the four-arm structure is formed between 2 and 5 kpc at $t \sim 30$ Myr, extending to larger radii at later times. But, after a ~ 300 Myr, while still the largest, the $m = 4$ mode is no longer dominant since other modes grow in the inner part of the galaxy. After $t \sim 150$ Myr, $A(4, r)$ is significant only in the $5 \text{ kpc} < R < 10 \text{ kpc}$ range, with its amplitude declining in time.

It is noticeable that the gas component in simulation I has the largest amplitudes, meaning that the gas is more tightly associated with a four-fold symmetric pattern than the stars. Comparing the stellar density in both simulations I and II, we may note that simulation II has larger $A(m, r)$ amplitudes, meaning that in the absence of gas, the spiral

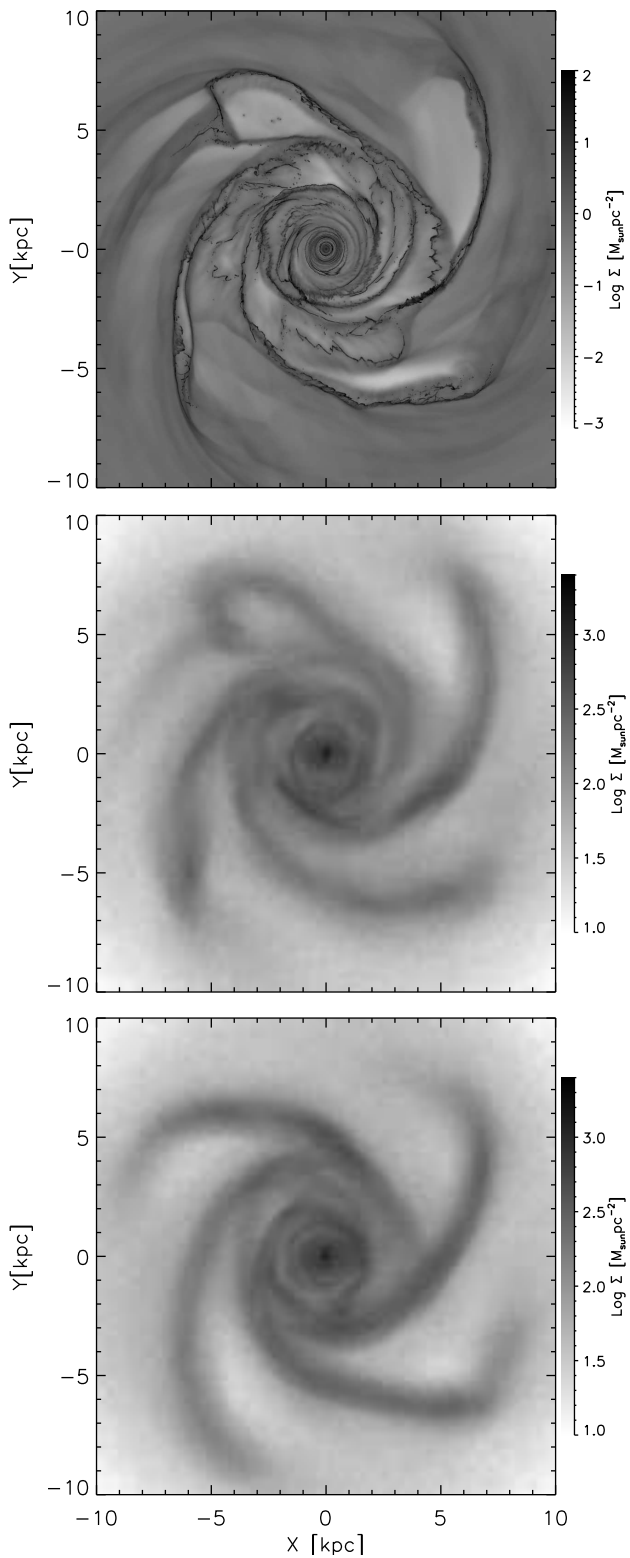


Figure 2. Gaseous (*top*) and stellar (*middle*) surface density distributions for simulation I, and stellar surface density (*bottom*) for simulation II at $t = 200$ Myr. For clarity, only the $r < 10$ kpc is shown.

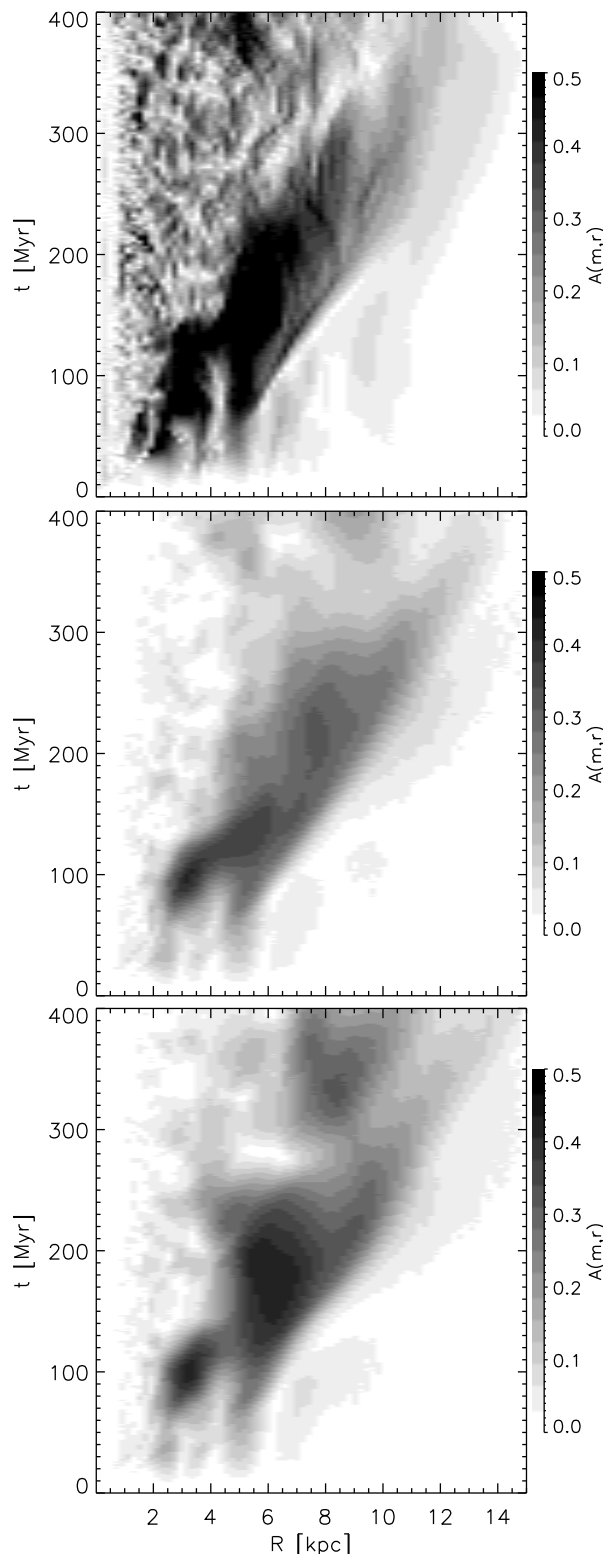


Figure 3. Evolution of the $m = 4$ mode for gas (*top*) and stars (*middle*) in simulation I, and stars (*bottom*) in simulation II.

structure is enhanced. One possible reason for this is that interactions between stars and giant molecular clouds heats the stellar disk, thus causing the spiral structure intensity to decrease. Since we failed to find a correlation between the stellar velocity dispersion and the gaseous disk surface density (for constant radius rings), we do not think this is the reason for a weaker spiral when gas is included. Another possible reason is that the spiral structure in simulation I is formed almost at the same time in the stellar and gaseous disks, but with a small phase difference (Shu et al. 1973, Pérez-Villegas, Gómez & Pichardo in prep.). Even if the gaseous arm is small compared to the stellar arm mass, this out-of-phase perturbation might cause a decrease on the stellar response.

In order to measure the pitch angle for each of the spiral modes that describe the density distribution, consider the amplitudes for the unwound modes,

$$\hat{A}(m, p) = \frac{1}{D} \int_{-\pi}^{+\pi} \int_{u_{min}}^{u_{max}} \Sigma(u, \phi) \exp[-i(m\phi + pu)] d\phi du, \quad (1)$$

where, $u = \log r$, m is the Fourier mode in question, $p = -m/\tan(\alpha)$ is a logarithmic wavenumber, α is the pitch angle of the spiral, Σ is the mass surface density distribution, and D is a normalization given by

$$D = \int_{-\pi}^{+\pi} \int_{r_{min}}^{r_{max}} \Sigma(u, \phi) du d\phi. \quad (2)$$

Figure 4 shows the amplitude $\hat{A}(m, p)$ for several m -values for both simulations. The $m = 4$ mode dominates the distribution for most of the evolution, and so, hence forth, we focus our analysis on this mode.

Figure 5 shows the evolution of $\hat{A}(4, p)$ during the simulation. In the plot it can be seen that, even if p remains almost constant, the amplitude $\hat{A}(m, p)$ changes in time. This might be explained if the spiral is formed by a superposition of transient waves that reinforce the pattern, as stated by Sellwood & Carlberg (2014), **or as a result of interference of longer-lived spiral waves, as proposed by Comparetta & Quillen (2012)**. For simulation I at 200 Myr, the stellar spiral is more open ($\alpha = 25.2^\circ$) than the gaseous one ($\alpha = 22.8^\circ$), in a similar fashion to simulations of gas in a fixed potential (Gómez et al. 2013). For simulation II, the pitch angle at $t = 200$ Myr is 29.7° , i.e., the simulation without a gaseous disk yields a more open spiral than the simulation with stars only. This values are consistent with a Sc galaxy (Ma 2002).

In order to determine the velocity of the spiral pattern, consider the amplitudes of the Fourier modes transformed again in time, as a function of radius, thus changing from (m, r, t) space to (m, r, Ω_p) . Consider the phase $\Phi = \arctan(A_{Im}/A_{Re})$ where A_{Im} and A_{Re} are the imaginary and the real parts of the amplitude. The pattern angular velocity is then given by $\Omega_p = \hat{\Phi}/N$, where $\hat{\Phi}$ is the Fourier transform in time of Φ and N is the total number of data outputs.

Figure 6 shows the so calculated spectrogram for the $m = 4$ component, along with the orbital frequency Ω of the (initial) axisymmetric disk. It is worth noting that, since the frequency resolution (the Nyquist frequency) is given by the time of the last data output, it is necessary to allow for the longest possible evolution of the simulation. In our case, Sim-

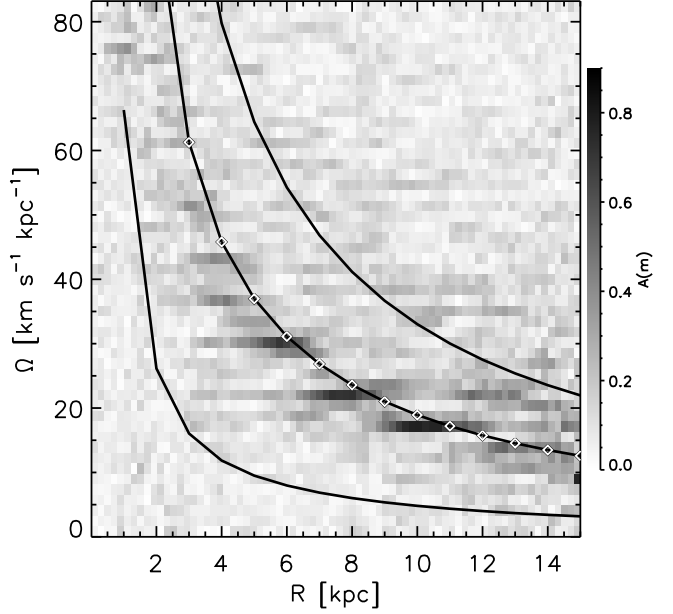


Figure 6. Spectrogram for the $m = 4$ mode in the stellar disk of simulation II for the length of the simulation, i.e., 923 Myr. The line with diamonds corresponds to the angular frequency for the axisymmetric disk, while the upper and lower lines represent the $\Omega \pm \kappa/4$ frequencies.

ulation I stopped due to numerical issues, but the Simulation II ran up to 923 Myr. So, the figure shows the spectrogram corresponding to the simulation with the stellar disk only, with 1 Myr between data outputs. As seen from the radial dependence of the amplitude maxima, the frequency for the spiral pattern is not constant but it is composed of a superposition of patterns with different frequencies constant on *restricted* radial ranges, in a manner consistent to the behavior reported by Sellwood & Carlberg (2014). This superposition of waves is also suggested in the time evolution shown in Figure 5. If Simulation I is used to measure the pattern speed, either with the stellar or gaseous disks, the lower frequency resolution smears these constant Ω_p regions, giving the impression that the spiral arms rotate solidly, similarly to those reported recently (Roca-Fàbrega et al. 2013; Grand et al. 2012b; Wada & Koda 2004; Wada et al. 2011).

4 SUMMARY

In this paper we performed SPH simulations of galactic disks using an SPH-Nbody code to model a disk with a gaseous and stellar components (simulation I) and a disk with stellar component only (II). The gaseous disk is modeled with an explicit cooling function, thus allowing it to segregate into dense and diffuse phases. We observed similar 4-arms structure in both simulations but, when a Fourier analysis is performed on the surface density distribution, the spiral structure in simulation II shows a higher $m = 4$ mode amplitude, with less substructure than simulation I, i.e., adding a gaseous component to the simulation leads to more substructure in both stellar and gaseous arms, but it also leads

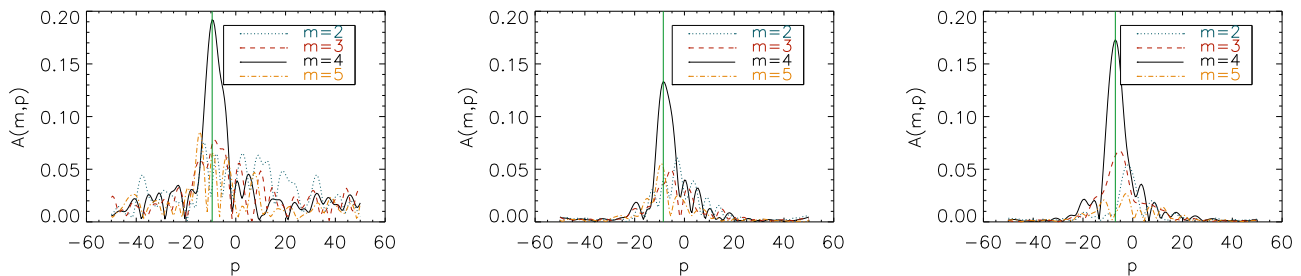


Figure 4. $\hat{A}(m, p)$ for gaseous disk for $t = 200$ Myr (*left*), for stellar disk $t = 200$ Myr (*center*) and stellar disk without gas (*right*). Lines represent different Fourier modes. The peak of the dominant $m = 4$ mode changes from p -values corresponding to pitch angles of $\alpha = 22.8^\circ$ (*left*), 25.2° (*center*) and 29.7° (*right*).

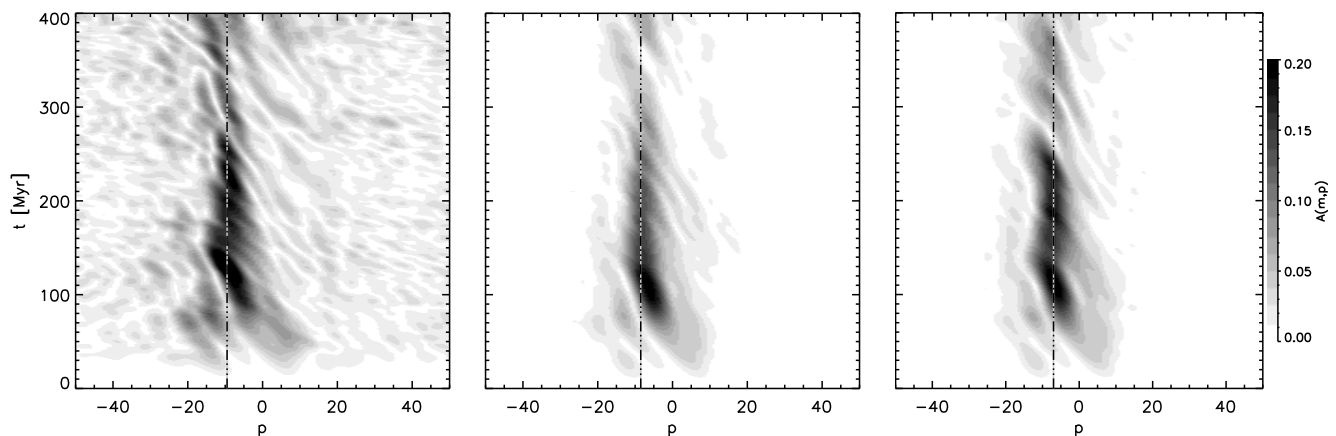


Figure 5. Time evolution of the logarithmic wavenumber, p . The maximum at each time indicate the pitch angle for the gaseous (*left*) and stellar disks (*center*) in simulation I, and the stellar disk in simulation II (*right*).

to a weaker stellar spiral. We speculate that this might be due to a phase shift between the gaseous and stellar arms, which reduces the coherence of the response to the non-axisymmetric part of the potential. This phase shift between stellar and gaseous spiral arms has been reported before in simulations with fixed spiral potentials (e.g. Shu et al. 1973; Gómez et al. 2013).

The simulations obtained were analyzed with a Fourier method to measure the pitch angle and the velocity of the spiral pattern. The spectrogram for simulation II shows that the pattern is better described as a superposition of waves, each with a constant pattern speed in a given radial range. Lack of frequency resolution smears the spectrogram and might make it appear as if the spiral pattern corotates with the disk, as the set of waves, as a whole, follows the rotation of the disk.

About the growth of spiral pattern, Figure 3 shows the evolution of the spiral structure in our simulations. It can be seen that, even if the spiral structure consists on small fluctuations, it grows globally in a coherent way. D’Onghia et al. (2013) shows that disconnected perturbations serve as seed for the growth of a global spiral pattern through swing amplification, which is favored by the particles’ self-gravity. In a similar way, over-densities in our simulations generate spiral

segments that connect and form a large-scale spiral pattern. The spiral consists on individual segments that rotate with distinct frequencies (as seen in fig. 6), but still a single global pattern emerge.

With respect to the pitch angles of the pattern, we measure $\alpha = 22.8^\circ$ for the gaseous disk, $\alpha = 25.2^\circ$ for the stellar disk in simulation I and $\alpha = 29.7^\circ$ for the stellar disk in simulation II. A gaseous spiral tighter than the stellar one has been reported in simulations before. But, the fact that the stellar spiral develops a larger pitch angle when the gas is absent appears counter-intuitive considering that the pitch angle is usually more open for disk galaxies of later Hubble type, which have a larger gas content. Further experiments with a range of structural parameters (namely bulge/disk mass ratio or disk/halo scale length ratio, for example) are necessary to explore the different ways the stellar and gaseous disks generate spiral structure in isolated galaxies.

ACKNOWLEDGMENTS

The authors wish to thank V. Debattista, E. D’Onghia, A. Pérez-Villegas, and J. Sellwood, for useful discussions on

the subject at hand and an anonymous referee for comments that greatly improved this manuscript. I.P. thanks the Mexican Foundation CONACyT for financial support. The numerical simulations were performed in the cluster at CRyA-UNAM acquired with CONACyT grants 36571-E and 47366-F to E. Vázquez-Semadeni. This work has received financial support from UNAM-DGAPA PAPIIT grant IN111313 to GCG.

REFERENCES

- Acreman D. M., Douglas K. A., Dobbs C. L., Brunt C. M., 2010, *MNRAS*, 406, 1460
- Allen C., Santillan A., 1991, *RevMexAA*, 22, 255
- Baba J., Saitoh T. R., Wada K., 2013, *ApJ*, 763, 46
- Bertin G., Lin C. C., 1996, *Spiral structure in galaxies a density wave theory*
- Comparetta J., Quillen A. C., 2012, *ArXiv e-prints*
- Davis B. L., Berrier J. C., Shields D. W., Kenefick J., Kenefick D., Seigar M. S., Lacy C. H. S., Puerari I., 2012, *ApJS*, 199, 33
- Dobbs C., Baba J., 2014, *ArXiv e-prints*
- D’Onghia E., Vogelsberger M., Hernquist L., 2013, *ApJ*, 766, 34
- Goldreich P., Lynden-Bell D., 1965, *MNRAS*, 130, 125
- Gómez G. C., Pichardo B., Martos M. A., 2013, *MNRAS*, 430, 3010
- Grand R. J. J., Kawata D., Cropper M., 2012a, *MNRAS*, 426, 167
- Grand R. J. J., Kawata D., Cropper M., 2012b, *MNRAS*, 421, 1529
- Jappsen A.-K., Klessen R. S., Larson R. B., Li Y., Mac Low M.-M., 2005, *A&A*, 435, 611
- Jog C. J., 1996, *MNRAS*, 278, 209
- Julian W. H., Toomre A., 1966, *ApJ*, 146, 810
- Koyama H., Inutsuka S.-I., 2000, *ApJ*, 1, 980
- Lin C. C., Shu F. H., 1964, *ApJ*, 140, 646
- Ma J., 2002, *A&A*, 395, 389
- Quillen A. C., Dougherty J., Bagley M. B., Minchev I., Comparetta J., 2011, *MNRAS*, 417, 762
- Roca-Fàbrega S., Valenzuela O., Figueras F., Romero-Gómez M., Velázquez H., Antoja T., Pichardo B., 2013, *MNRAS*, 432, 2878
- Sellwood J. A., Carlberg R. G., 2014, *ApJ*, 785, 137
- Shu F. H., Milione V., Roberts Jr. W. W., 1973, *ApJ*, 183, 819
- Springel V., Yoshida N., White S., 2001, *New Astronomy*, 6, 79
- Vallée J. P., 2005, *AJ*, 130, 569
- Vázquez-Semadeni E., Gómez G. C., Jappsen A. K., Ballesteros-Paredes J., González R. F., Klessen R. S., 2007, *ApJ*, 657, 870
- Wada K., Baba J., Saitoh T. R., 2011, *ApJ*, 735, 1
- Wada K., Koda J., 2004, *MNRAS*, 349, 270